

Facile sensitizing of PbSe film for near-infrared photodetector by microwave plasma processing

Kangyi Zhao(赵康伊), Shuanglong Feng(冯双龙), Chan Yang(杨婵),Jun Shen(申钧), and Yongqi Fu(付永启)
Citation: Chin. Phys. B, 2022, 31 (**3**): 038504. DOI: 10.1088/1674-1056/ac3224
Journal homepage: http://cpb.iphy.ac.cn; http://iopscience.iop.org/cpb
What follows is a list of articles you may be interested in

Graphene-based heterojunction for enhanced photodetectors

Haiting Yao(姚海婷), Xin Guo(郭鑫), Aida Bao(鲍爱达), Haiyang Mao(毛海央),Youchun Ma(马游春), and Xuechao Li(李学超)
Chin. Phys. B, 2022, 31 (**3**): 038501. DOI: 10.1088/1674-1056/ac1b8b

Dual-wavelength ultraviolet photodetector based on vertical (Al,Ga)N nanowires and graphene

Min Zhou(周敏), Yukun Zhao(赵宇坤), Lifeng Bian(边历峰), Jianya Zhang(张建亚), Wenxian Yang(杨文献), Yuanyuan Wu(吴渊渊), Zhiwei Xing(邢志伟), Min Jiang(蒋敏), and Shulong Lu(陆书龙)
Chin. Phys. B, 2021, 30 (**7**): 078506. DOI: 10.1088/1674-1056/abff23

Deep-ultraviolet and visible dual-band photodetectors by integrating Chlorin e6 with Ga_2O_3

Yue Zhao(赵越), Jin-Hao Zang(臧金浩), Xun Yang(杨珣), Xue-Xia Chen(陈雪霞), Yan-Cheng Chen(陈彦成), Kai-Yong Li(李凯永), Lin Dong(董林), and Chong-Xin Shan(单崇新)
Chin. Phys. B, 2021, 30 (**7**): 078504. DOI: 10.1088/1674-1056/abf91c

A method to extend wavelength into middle-wavelength infrared based on InAsSb/(Al)GaSb interband transition quantum well infrared photodetector

Xuan-Zhang Li(李炫璋), Ling Sun(孙令), Jin-Lei Lu(鲁金蕾), Jie Liu(刘洁), Chen Yue(岳琛), Li-Li Xie(谢莉莉), Wen-Xin Wang(王文新), Hong Chen(陈弘), Hai-Qiang Jia(贾海强), Lu Wang(王禄)
Chin. Phys. B, 2020, 29 (**3**): 038504. DOI: 10.1088/1674-1056/ab6969

Performance of dual-band short- or mid-wavelength infrared photodetectors based on InGaAsSb bulk materials and InAs/GaSb superlattices

Yao-yao Sun(孙姚耀), Yue-xi Lv(吕粤希), Xi Han(韩玺), Chun-yan Guo(郭春妍), Zhi Jiang(蒋志), Hong-yue Hao(郝宏玥), Dong-wei Jiang(蒋洞微), Guo-wei Wang(王国伟), Ying-qiang Xu(徐应强), Zhi-chuan Niu(牛智川)
Chin. Phys. B, 2017, 26 (**9**): 098506. DOI: 10.1088/1674-1056/26/9/098506

Facile sensitizing of PbSe film for near-infrared photodetector by microwave plasma processing

Kangyi Zhao(赵康伊)[1], Shuanglong Feng(冯双龙)[2,†], Chan Yang(杨婵)[2], Jun Shen(申钧)[2], and Yongqi Fu(付永启)[1,‡]

[1] *School of Physics, University of Electronic Science and Technology of China, Chengdu* 610054, *China*
[2] *Chongqing Institute of Green and Intelligent Technology, Chinese Academy of Sciences, Chongqing* 400714, *China*

(Received 9 March 2021; revised manuscript received 23 September 2021; accepted manuscript online 22 October 2021)

High quality PbSe film was first fabricated by a thermal evaporation method, and then the effect of plasma sensitization on the PbSe film was systemically investigated. Typical detectivity and significant photosensitivity are achieved in the PbSe-based photodetector, reaching maximum values of 7.6×10^9 cm·Hz$^{1/2}$/W and 1.723 A/W, respectively. Compared with thermal annealing, plasma sensitization makes the sensitization easier and significantly improves the performance.

Keywords: PbSe film, infrared photodetector, plasma processing

PACS: 77.55.–g, 07.57.–c, 52.77.Dq **DOI:** 10.1088/1674-1056/ac3224

1. Introduction

PbSe is a typical narrow bandgap semiconductor material with full application in infrared detectors.[1–5] For photodetectors, high quality PbSe film has been successfully fabricated by chemical bath deposition,[6] electrochemical deposition,[7] thermal evaporation,[8] and molecular beam epitaxy method[9] during the past two decades. When making devices from materials, it is often necessary to sensitize PbSe under an oxygen/halogen atmosphere to improve the stability of devices and reduce noise, which is a critical process that determines the performance of photodetectors.[10–15] For a long time, scientists worldwide have researched the sensitization method and sensitization mechanism of PbSe based devices.[16–19] For example, Humphrey and Scanlon reported that the p–n type of PbSe film can be converted by doping the halogen group during thermal sensitization.[20] Zhao *et al.* introduced a charge separation junction model to further explain the sensitization mechanism of the PbSe photodetector.[21] However, studies on plasma as the sensitization method of PbSe thin film are relatively few.

In this work, the higher-reaction active ground states of microwave plasma were utilized to sensitize the PbSe thin film.[22–26] The morphology, crystal structure, and elemental composition of the sample before and after plasma processing were investigated in detail. By comparing the performance of photodetectors, the detectivity (D^*) of a plasma-sensitizing PbSe-based device is found to be 17.5 times better than that of the raw materials. Finally, the mechanism of plasma sensitization is also discussed based on the Hall effect test.

2. Experimental details

2.1. Materials synthesis and sensitizing

The 500 nm PbSe thin film was deposited on Si/SiO_2 substrates by a thermal evaporation method. Before deposition, the Si/SiO_2 substrates were ultrasonically cleaned with acetone, deionized water, and ethanol in sequence. High-purity PbSe powder (99.99%) was loaded in a graphite crucible with a crucible/substrate distance of about 26 cm in the vacuum chamber. The substrate temperature was set to 200 °C and the vacuum pressure was about 5.5×10^{-4} Pa. Subsequently, the PbSe film was processed in a homemade microwave plasma chemical vapor deposition (MPCVD) process consisting of a domestic microwave oven (with the power set at 700 W, 2.45 GHz), a gas supply system, a quartz tube (25 mm outer diameter) and a vacuum pump. Gaseous Ar_2 (70 sccm) flowed into the quartz tube accompanied by continuous pumping and maintained at a base pressure of about 10^{-1} Pa. Then, Ar plasma with bright purple color was generated when the microwave was turned on. Finally, the microwave oven/gas valve was closed and the treated sample was taken out.

2.2. Material characterization

The crystal structure of the film was identified by an x-ray diffractometer (XRD, Bruker D8-Focus). The surface morphology and elemental composition of the film were characterized by a scanning electron microscope (SEM, Shimadzu, SSX-550) equipped with energy-dispersive spectroscopy (EDS). The optical properties (absorption and reflectivity) of the film were recorded using a near-infrared (NIR) spectrophotometer (Gangdong, S410).

†Corresponding author. E-mail: fengshuanglong@cigit.ac.cn
‡Corresponding author. E-mail: yqfu@uestc.edu.cn

© 2022 Chinese Physical Society and IOP Publishing Ltd

2.3. Photoresponse measurement

Both the *I*–*V* characteristics and photoresponses of the fabricated devices were recorded by a Keithley 4200 source meter at room temperature. Photoresponse measurement was carried out at a laser wavelength of 1550 nm, and the current was measured while the illumination was modulated between on and off with a shutter controlled by a square wave signal. To further evaluate the photodetector performance of the PbSe film via Ar plasma by MPCVD equipment, a PbSe-based photoconductor was fabricated on a SiO_2/Si substrate (0.4 cm × 0.2 cm). In this structure, photolithography patterns were formed by photolithography (shadow-mask-used). An ohmic contact with Cr/Au (3 nm/50 nm) electrodes was realized by e-beam deposition and standard lift-off process; the effective photoactive area of PbSe was 0.2 cm × 0.2 cm.

3. Results and discussion

Figure 1(a) shows the XRD patterns of the thermally evaporated PbSe films as a function of plasma handling time. The diffraction peaks correspond to the (110), (111), (200), (012), (220), (311), (400), and (204) planes, which can be indexed to the cubic PbSe phase in good agreement with the JCPDS card 06-0354. Although some oxide diffraction peaks appear in the diffraction pattern, the PbSe diffraction peaks are still dominant, such as the (200)-serial diffraction peak. This indicates that the interior of the grain is still PbSe, and only the surface layer of the PbSe grain is partially oxidized. The predominant (200)-serial diffraction peaks are observed for all samples, the intensities of which are enhanced with increasing microwave time. This behavior should be attributed to the improvement in the corresponding diffraction orientations. The full width at half maximum (FWHM, denoted as β) of the (200) peak, which has been calibrated by deducting the instrumental broadening, decreases with increasing microwave time until reaching a minimum value at 6 min, and then increases with a continuous increase in plasma handling time. This reveals that the crystallinity of the films is improved with increasing microwave time, reaching a maximum at 6 min. Subsequently, the absorptivity of PbSe films with different plasma handling times is also investigated, as shown in Fig. 1(b). It indicates that the infrared absorptivity did not change significantly under different microwave treatment times, fluctuating within 62%–72%, with the lowest absorptivity at 8 min under microwave treatment. Finally, the atomic ratios of Pb, Se, O, and Si are obtained by EDS, as shown in Fig. 1(c). During the plasma treatment (0–8 min), the atomic ratio of Pb and Se is approximately 1:1; the proportion of O atom decreases

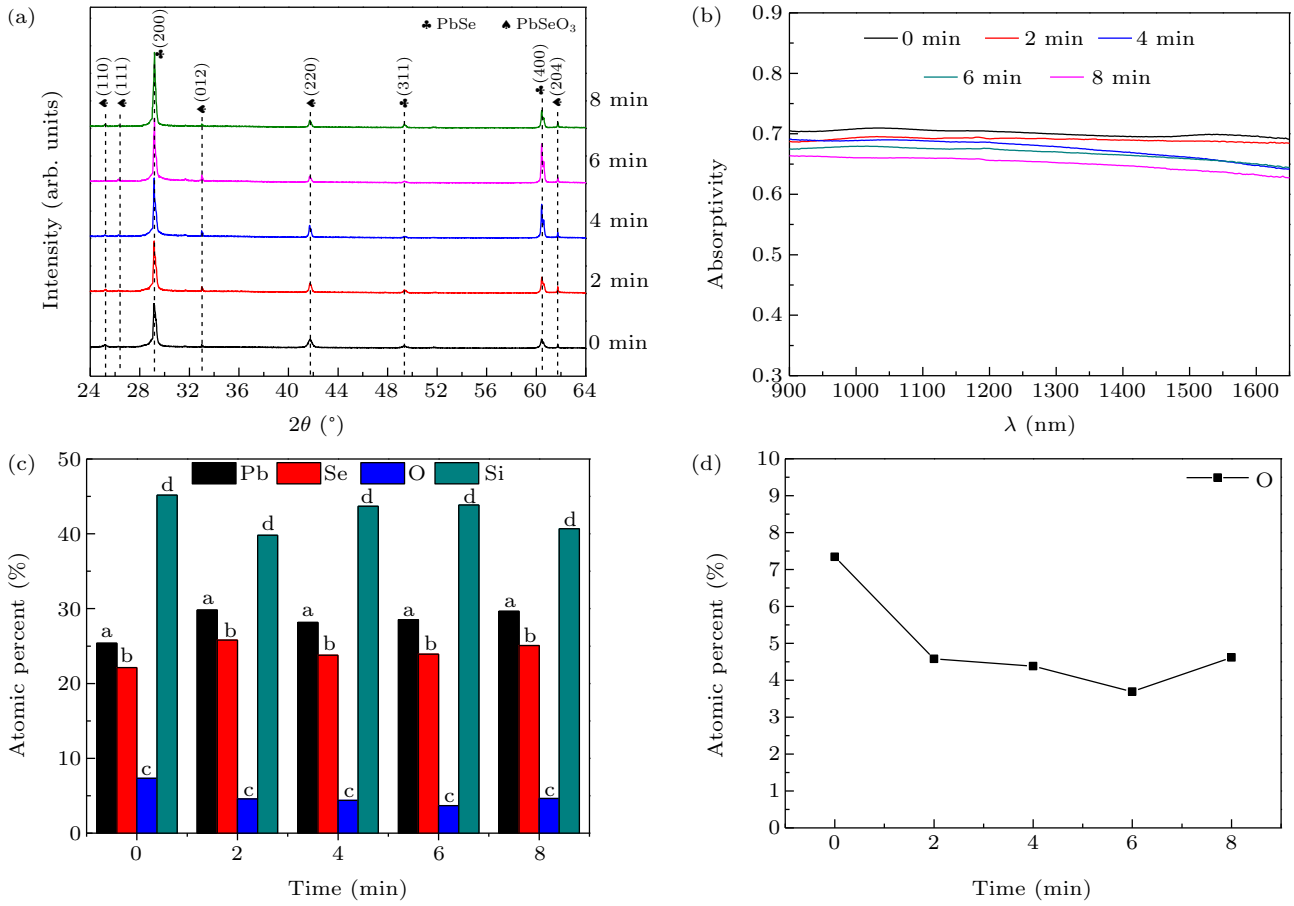


Fig. 1. (a) XRD patterns of PbSe film with different microwave processing times; (b) optical absorption spectrum of the PbSe film under different microwave processing times; (c) atomic ratios of Pb, Se, O, and Si as a function of time plotted in the histogram; (d) content curve of O element in the samples under different handling times.

slightly compared with no plasma treatment, but the O atom proportion changes little as the subsequent plasma processing time increases from 2 min to 8 min as shown in Fig. 1(d). It is reasonable that plasma treatment causes a sintering phenomenon in the PbSe thin film and improves the degree of crystallization.

The SEM images of the PbSe film with different plasma handling times are illustrated in Fig. 2. For the PbSe film with plasma handling time $t = 0$ min in Fig. 2(a), the PbSe thin film is composed of particles agglomerated by nanocrystals, and the film layer is continuous with a dense structure. With the treatment of Ar plasma for 2 min, the PbSe film is no longer granular and presents features of high crystal quality, dense structure, and excellent uniformity, as shown in Fig. 2(b). The crystallinity of the PbSe thin film continues to increase with increasing microwave plasma action time until some holes appear on the thin film under the etching process of Ar ions. With the increase in etching time, an increasing number of holes are found in the film, as shown in Figs. 2(c)–2(e).

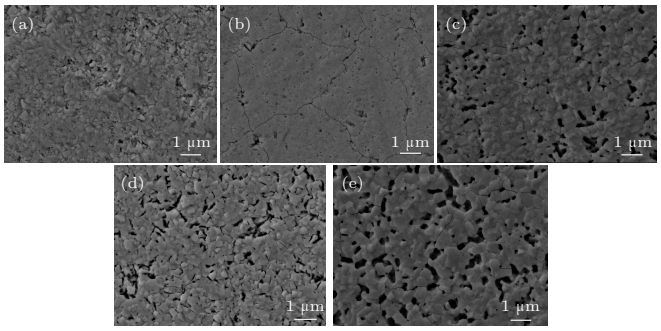


Fig. 2. SEM image of treated PbSe film: (a) 0 min; (b) 2 min; (c) 4 min; (d) 6 min; (e) 8 min.

Figure 3(a) is the actual product of the PbSe NIR photodetector, and the PbSe thin film device in the photodetector is shown in Fig. 3(b). The manufacturing method of the PbSe device is to prepare PbSe thin film and Au electrodes on a Si/SiO_2 substrate, where the size of the SiO_2/Si substrate is 4 cm × 2 cm, the size of the electrode is 1 cm × 2 cm, and the size of the PbSe thin film is 2 cm × 2 cm, as shown in Fig. 3(b). We use a Keithley 4200 source meter for testing and plot the corresponding photoresponse spectrum as shown in Figs. 4(b)–4(f). Figure 4(a) is the schematic diagram of the PbSe photodetector for the 4200 photoresponse spectrum test, where the thickness of the SiO_2/Si substrate is 300 μm, and the electrode is composed of Cr (3 nm) and Au (50 nm). Figures 4(b)–4(f) depicts the dynamic properties of the fabricated PbSe photodetector at a bias voltage of 10 V at different plasma handling time; the photocurrents of the different samples are respectively 1.9×10^{-5} A (0 min), 1.0×10^{-4} A (2 min), 1.38×10^{-4} A (4 min), 2.79×10^{-4} A (6 min), and 1.6×10^{-4} A (8 min). We calculate the responsivity (R) and the detectivity (D^*) based on the photoresponse spectrum to evaluate the performance of the PbSe photodetector. The responsivity (R) is calculated as $R = I_{\text{photo}}/P_{\text{opt}}$, and $P_{\text{opt}} = (P_{\text{light}} \times A_{\text{detect}})/A_{\text{spot}}$, where I_{photo} is the photocurrent under illumination, P_{opt} is the optical power of incident infrared radiation, P_{light} is the incident power ($P_{\text{light}} = 5 \times 10^{-4}$ W), A_{spot} is the laser-beam-illuminated device area, and A_{detect} is the actual effective detection area of the device. Hence, the responsivity (R) is calculated as 0.12 A/W (0 min), 0.629 A/W (2 min), 0.868 A/W (4 min), 1.723 A/W (6 min), and 1.006 A/W (8 min). The detectivity (D^*) is defined as $D^* = R \times \sqrt{A}/\sqrt{2qI_{\text{dark}}}$, where q is the absolute value of electron charge, R is the responsivity and the dark currents of the different samples are respectively 9.487×10^{-3} A (0 min), 6.886×10^{-3} A (2 min), 6.436×10^{-3} A (4 min), 6.434×10^{-3} A (6 min), and 6.038×10^{-3} A (8 min). Thus, the detectivity (D^*) is calculated as 4.338×10^8 cm·Hz$^{1/2}$/W (0 min), 2.68×10^9 cm·Hz$^{1/2}$/W (2 min), 3.925×10^9 cm·Hz$^{1/2}$/W (4 min), 7.6×10^9 cm·Hz$^{1/2}$/W (6 min), and 4.58×10^9 cm·Hz$^{1/2}$/W (8 min). The rising and decaying time values in a single on/off cycle are plotted in Figs. 5(a)–5(d).

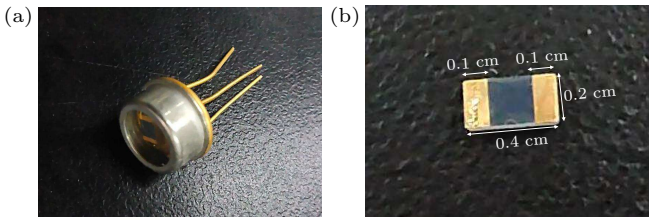


Fig. 3. (a) PbSe photodetector with a microwave time of 6 min; (b) PbSe device with dimensions.

In summary, we present the responsivity (R), detectivity (D^*) and response time under different microwave times in Table 1 for comparative analysis. As shown in Table 1, with an increase in microwave treatment time, the responsivity (R) and detectivity (D^*) of the PbSe devices first increase and decrease. When the microwave treatment time is 6 min, the responsivity (R) and detectivity (D^*) of the device reach their maxima, respectively 1.723 A/W and 7.6×10^9 cm·Hz$^{1/2}$/W. At this time, the response time of the PbSe device is also the fastest. The rising time value and falling time value of the sampling interval are 4 μs and 2 μs, respectively. The response time of the PbSe device is two orders of magnitude lower than those of PbSe devices with other microwave treatment times, and the response time is significantly reduced. Thus, the responsivity (R) and detectivity (D^*) are the largest, and the response time is shortest at the plasma treatment time $t = 6$ min, which is the optimal sensitization condition. For practical utility, we directly measure using a fast Fourier transform (FFT) spectrum analyzer because the noise property is determined mainly by dark current. The current measured directly using the FFT method is much more credible. We obtain the I–V curve (dark current/1550 nm)

and voltage noise spectral density under the optimal sensitization condition, as shown in Figs. 6(a) and 6(b). It can be seen from Fig. 6(a) that whether the photocurrent or dark current of the device passes through the origin of the coordinate, it can be judged that the PbSe infrared photodetector is ohmic contact, and the contact is good. $R = 1594\ \Omega$ ($t = 6$ min, $\lambda = 1550$ nm), $\chi = -142.8$ dB·V/Hz$^{1/2}$ when frequency $f = 1$ Hz from Figs. 6(a) and 6(b). The noise current is $I_n = V_0/R = 10^{\chi/20}/R = 5 \times 10^{-8}$ A/Hz$^{1/2}$. The noise property in this device is determined mainly by dark current. D^* represents the ability of the device to detect weak light signals and can be obtained by the formula $D^* = R \times \sqrt{A}/I_n$, where A is the effective area of the device (2 cm × 2 cm), I_n is the noise current, and $D^* = 6.892 \times 10^9$ cm·Hz$^{1/2}$/W. Thus, considering noise interference, the detectivity (D^*) is 6.892×10^9 cm·Hz$^{1/2}$/W in practical application.

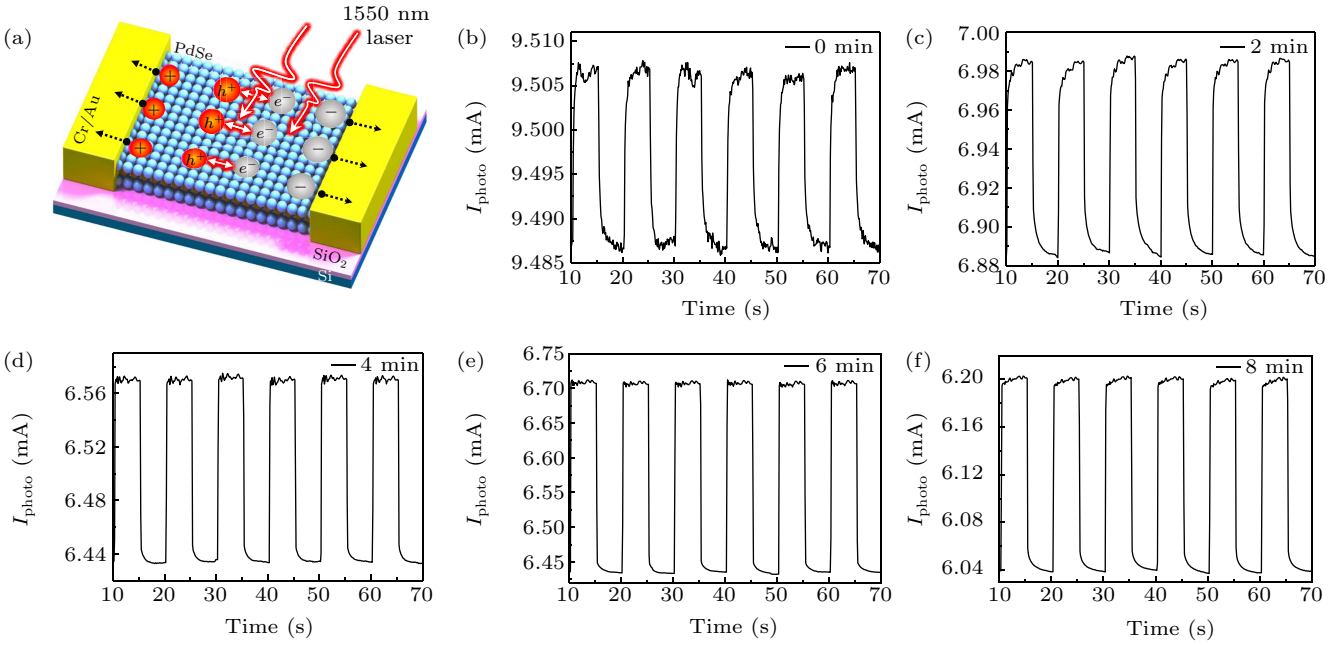


Fig. 4. (a) Schematic of the PbSe photodetector; photoresponse spectra under the illumination of $\lambda = 1550$ nm at different microwave processing times (bias voltage is 10 V): (b) 0 min; (c) 2 min; (d) 4 min; (e) 6 min; (f) 8 min.

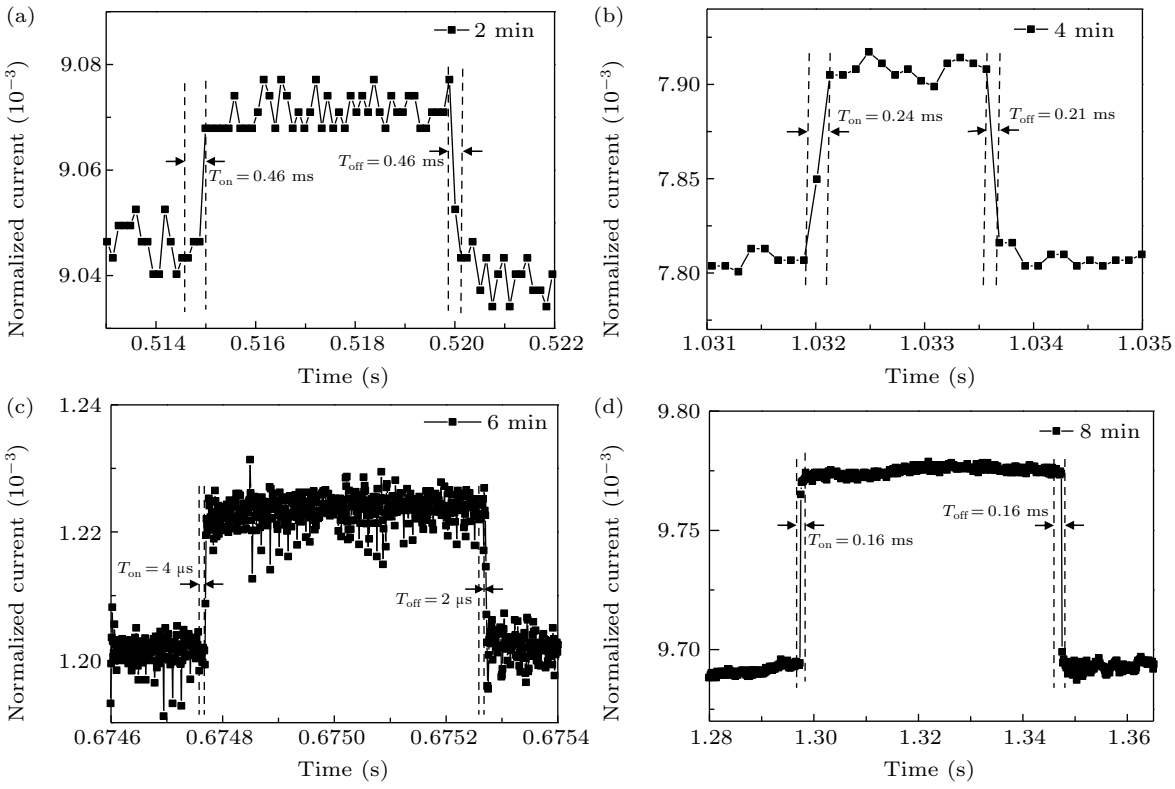


Fig. 5. Response time diagram at different microwave processing times: (a) 2 min; (b) 4 min; (c) 6 min; (d) 8 min.

Table 1. Responsivity (R), detectivity (D^*) and response time data list at different plasma time.

Time (min)	Photocurrent (A)	Responsivity (A/W)	Detectivity (cm·Hz$^{1/2}$/W) (calculated)	Response time (on) (ms)	Response time (off) (ms)
0	1.9×10^{-5}	0.120	4.338×10^{8}	–	–
2	1.0×10^{-4}	0.629	2.68×10^{9}	0.46	0.35
4	1.38×10^{-4}	0.868	3.825×10^{9}	0.24	0.14
6	2.79×10^{-4}	1.723	7.6×10^{9}	0.004	0.002
8	1.6×10^{-4}	1.006	4.58×10^{9}	0.16	0.16

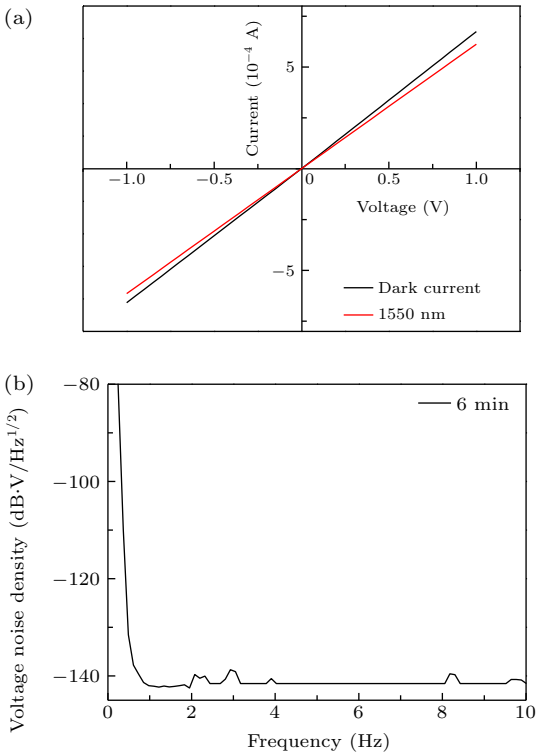


Fig. 6. (a) The I–V curve of the PbSe photodetector with microwave time t = 6 min (dark current/1550 nm); (b) voltage noise spectral density measured at plasma time t = 6 min.

We analyzed the performance of the PbSe photodetector under the optimal sensitization condition t = 6 min. We obtained the photoresponse spectra of the PbSe films as a function of voltage and the photocurrent of the PbSe films as a function of optical power, as shown in Figs. 7(a) and 7(b). As can be seen in Fig. 7(a), the microwave processing time is 6 min and the incident light wavelength is 1550 nm. When the power of the light source is stable, the device photocurrent increases with an increase in the bias voltage. When the power of the incident light source is constant, the number of carriers generated per unit area of the film surface is constant. In this case, the greater the bias voltage, the more carriers can be effectively separated by the device, so the photocurrent of the device is larger. When the bias voltage of the test system is 10 V, $Y = 0.06163X + 2.3985\times10^{-4}$. Because the system bias voltage is constant, increasing the power of the incident light source increases the number of photogenerated carriers generated per unit area of the film and the device generates a larger photocurrent. The PbSe infrared photodetector experimental result is consistent with the theoretical analysis, indicating that the device meets expectations.

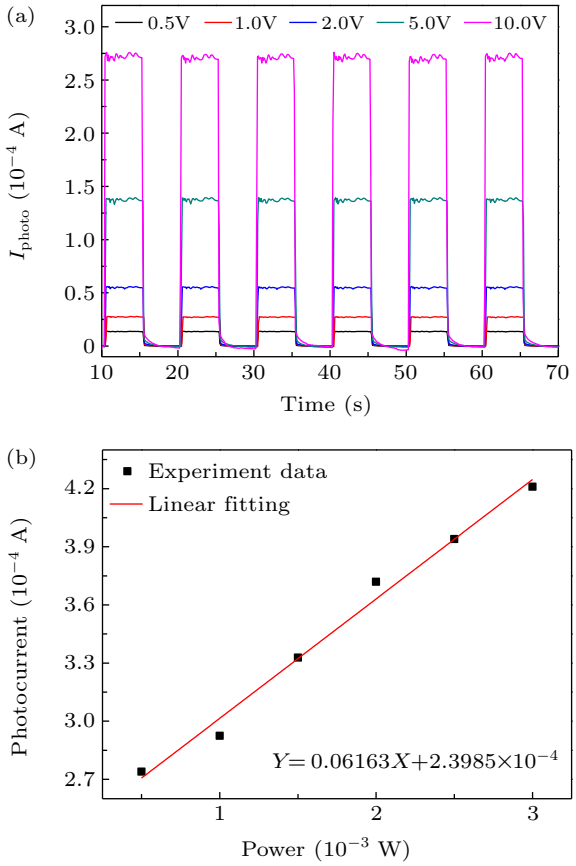


Fig. 7. (a) Photoresponse spectra of PbSe film as a function of voltage under the illumination of λ = 1550 nm ($P_{light} = 5\times10^{-4}$ W); (b) photocurrent of PbSe film as a function of optical power (U = 10 V).

A Hall effect tester (L79/HCS) is used to test the Hall coefficient, carrier concentration, migration rate, and conductivity to understand the change in the plasma-processed photodetector. The results are shown in Table 2. The positive Hall coefficient indicates that the PbSe film before and after plasma processing is p-type. As the action time of Ar plasma increases, the conductivity and the migration rate of the PbSe film initially gradually increase and then decrease, reaching a maximum when the plasma treatment time is 6 min. At this time, the conductivity of the PbSe thin film is 0.06872 Ω·cm, and the migration rate of the PbSe film is 11.553 cm^2/(V·s). The photoelectric performance is best when the responsivity (R) and detectivity (D^*) of the PbSe film are at a maximum.

In summary, the PbSe layer as a volatile precursor participates in a chemical reaction during the MPCVD process; Ar plasma diffuses from the surface of the PbSe thin film to the inside and reacts with the PbSe film, resulting in a secondary deposition on the PbSe layer itself, which improves the photoelectric performance of the PbSe film significantly.

Table 2. Test results of PbSe thin film Hall effect.

Time (min)	Hall coefficient (cm^3/C)	Carrier concentration (cm^2)	Migration rate ($cm^2/(V·s)$)	Conductivity (Ω·cm)
0	8.001	7.81×10^{17}	0.174	0.0218
2	30.273	2.06×10^{17}	0.894	0.029 53
4	131.680	4.75×10^{16}	4.469	0.033 94
6	168.164	3.88×10^{16}	11.553	0.068 72
8	237.227	2.64×10^{16}	9.75	0.041 10

4. Conclusion

In summary, PbSe thin film was fabricated by a thermal evaporation method, and Ar plasma realized the sensitization of a PbSe photodetector. The responsivity and detectivity of the PbSe photoconductor can be improved by an order of magnitude after quick plasma sensitization. The detectivity of a plasma sensitizing PbSe based devices is 17.5 times better than that of the raw materials. The response time reaches the magnitude of microseconds, providing a potential method of fabricating high-performance PbSe-based optoelectronic detectors.

Acknowledgments

Project supported by the National Natural Science Foundation of China (Grant Nos. 61605207, 61704172, and 61705229), the Key Research and Development Plan of the Ministry of Science and Technology of China (Grant No. 2017YFE0131900), the Western Light Program of the Chinese Academy of Sciences, and Youth Innovation Promotion Association of Chinese Academy of Sciences (Grant No. 2018416).

References

[1] Wu D, Guo J, Du J, Xia C, Zeng L, Tian Y, Shi Z, Tian Y, Li X J, Tsang Y H and Jie J 2019 *ACS Nano* **13** 9907
[2] Wu D, Jia C, Shi F, Zeng L, Lin P, Dong L, Shi Z, Tian Y, Li X and Jie J 2020 *J. Mater. Chem. A* **8** 3632
[3] Yang C, Zhou D H, Yang J, Tang L L, Leng C Q and Shen J 2020 *Phys. E* **124** 114216
[4] Li Q, Chen X S and Lu W 2019 *Acta Phys. Sin.* **68** 120701 (in Chinese)
[5] Zheng J J, Wang Y R, Yu K H, Xu X X, Sheng X X, Hu E T and Wei W 2018 *Acta Phys. Sin.* **67** 118502 (in Chinese)
[6] Khan A U and Kasha M 1979 *Proc. Natl. Acad. Sci. USA* **76** 6047
[7] Ivanou D K, Ivanova Y A, Poznyak S K, Starykevich M, Ferreira M, Mendes A and Streltsov E A 2017 *Electrochim. Acta* **249** 369
[8] Torquemada M C, Villamayor V, Rodrigo M T, Vergara G, Sanchez F J, Almazan R, Verdu M, Rodriguez P, Gomez L J and Montojo T M 2003 *Infrared Technol. Appl. XXIX* **5074** 592
[9] Weng B, Zhao F, Ma J, Yu G, Xu J and Shi Z 2010 *Appl. Phys. Lett.* **96** 251911
[10] Muñoz A, Meléndez J, Torquemada M C, Rodrigo M T, Cebrián J, De Castro A J, Meneses J, Ugarte M, López F, Vergara G, Hernández J L, Martín J M, Adell L and Montojo M T 1998 *Thin Solid Films* **317** 425
[11] Sierra C, Torquemada M C, Vergara G, Rodrigo M T, Gutiérrez C, Pérez G, Génova I, Catalán I, Gómez L J, Villamayor V, Ávarez M, Fernández D, Magaz M T and Almazán R M 2014 *Sens. Actuators B: Chem.* **190** 464
[12] Kumar P, Pfeffer M, Berthold C and Eibl O 2018 *J. Alloys Compd.* **735** 1654
[13] Weng B, Qiu J, Zhao L, Yuan Z, Chang C and Shi Z 2014 *Appl. Phys.* **104** 121111
[14] McDowell L L, Qiu J, Weng B and Shi Z 2019 *Cryst. Growth Des.* **19** 2253
[15] Yang H, Li X, Wang G and Zheng J 2018 *Coatings* **8** 444
[16] Ren Y, Dai T, He B and Liu X 2019 *Mater. Lett.* **236** 194
[17] Zhu T, Zheng L, Yao X, Liu L, Huang F, Cao Y and Gong X 2019 *ACS Appl. Mater. Interfaces* **11** 9205
[18] Ghorban Shiravizadeh A, Elahi S M, Sebt S A and Yousefi R 2018 *J. Appl. Phys.* **123** 083102
[19] Ren Y X, Dai T J, Luo W B and Liu X Z 2018 *J. Alloys Compd.* **753** 6
[20] Humphrey J N and Petritz R L 1957 *Phys. Rev.* **105** 1736
[21] Zhao L, Qiu J, Weng B, Chang C, Yuan Z and Shi Z 2014 *J. Appl. Phys.* **115** 084502
[22] Shivkumar G, Tholeti S S, Alrefae M A, Fisher T S and Alexeenko A A 2016 *J. Appl. Phys.* **119** 113301
[23] Meyyappan M 2009 *J. Phys. D: Appl. Phys.* **42** 213001
[24] Liu Y, Jiang G, Sun S, Xu B, Zhou J, Zhang Y and Yao J 2017 *J. Electroanal. Chem.* **804** 212
[25] Kar R, Patel N N, Chand N, Shilpa R K, Dusane R O, Patil D S and Sinha S 2016 *Carbon* **106** 233
[26] Corona-Gomez J, Shiri S, Mohammadtaheri M and Yang Q 2017 *Surf. Coatings Technol.* **332** 120